

Side Information in Robust Principle Component Analysis: Algorithms and Applications

Niannan Xue Yannis Panagakis Stefanos Zafeiriou
 Imperial College London, UK
 {n.xue15,i.panagakis,s.zafeiriou}@imperial.ac.uk

Abstract

Robust rank minimisation aims at recovering a low-rank subspace from grossly corrupted high-dimensional (often visual) data and is a cornerstone in many machine learning and computer vision applications. The most prominent method for this task is the Robust Principal Component Analysis (PCA). It recovers a low-rank matrix from sparse corruptions of unknown magnitude and support by Principal Component Pursuit (PCP), which is a convex approximation to the otherwise NP-hard rank minimisation problem. Even though PCP has been shown to be very successful in solving many rank minimisation problems, there are cases where degenerate or suboptimal solutions are obtained. This can be attributed to the fact that domain-dependent prior knowledge is not taken into account by PCP. In this paper, we address the problem of PCP when prior information is available. To this end, we propose algorithms for solving the PCP problem with the aid of prior information on the low-rank structure of the data. The versatility of the proposed methods is demonstrated by applying them to four applications, namely background subtraction, facial image denoising, face and facial expression recognition. Experimental results on synthetic and five real world datasets indicate the robustness and effectiveness of the proposed methods on these application domains, largely outperforming previous approaches that incorporate side information within Robust PCA.

1. Introduction

Principal Component Pursuit as proposed in [9] and its variants *e.g.* [2, 10, 11, 12, 30] are the current methods of choice for recovering a row-rank subspace from a set of grossly corrupted, possibly incomplete high-dimensional data. The above PCP-like methods employ the nuclear norm (*i.e.* the convex surrogate of the rank constraint) and the resulting convex relaxation has been shown to be very successful in solving many rank minimisation problems. In

particular, under certain conditions (such as the restricted isometry property [8]), the relaxation gap is zero, and rank minimisation is equivalent to nuclear norm minimisation. However, these conditions rarely hold for real world visual data and PCP yields degenerate or suboptimal solutions. To alleviate this, domain-dependent prior knowledge can be taken into account by PCP.

Indeed, in many applications knowledge regarding the low-rank component, albeit noisy, could be available. For instance, in background subtraction we may find some frames of the video that do not contain changes and therefore we may use them to accurately estimate the background. Another example concerns the problem of disentangling identity and expression components in expressive faces, where the low-rank component is roughly similar to the available neutral face. This paper is concerned with the problem of using a *noisy* approximation of the low-rank component to drive PCP, a problem that, to the best of our knowledge, has not been studied before.

The use of side information has been studied in related problems, such as matrix completion [16, 19] and compressed sensing [15]. More recently, side information has been studied in the PCP framework in the *noiseless* case. That is, the prior information regarding the low-rank subspace is supposed to be noise-free. Specifically, in [7] an orthogonal column space was used in order to drive a PCP-based deformable image alignment algorithm. In other words, the low-rank space was always written as a linear combination of the given column space. A more general approach was recently proposed in [17] where both a column and a row space were provided as side information and the algorithm had to recover the weights of the interaction between the column and the row space. Disappointingly, methods such as [7] and [17] generally require a set of clean, noise-free data samples in order to determine the column and/or row spaces of the low-rank component. Clearly, such data are difficult to find in practice.

In this paper, inspired by the recent work on compressed sensing [15], we propose a novel methodology for exploiting possibly noisy side information in PCP. In particular,

our contributions are summarised as follows:

- A novel PCP model using side information is proposed. More specifically, we propose a convex program that takes into account a possibly noisy approximation of the low-rank component in order to derive the accurate and meaningful low-rank component.
- Furthermore, we extend our proposed PCP model using side information to exploit prior knowledge regarding the column and row spaces of the low-rank components in a more general algorithmic framework.
- We demonstrate the usefulness of the proposed approaches in several applications, including background subtraction, facial image denoising as well as face recognition and facial expression classification by disentangling identity and expression components in an unsupervised way.

2. Related work

We first introduce the notations used throughout the paper. Lowercase letters denote scalars and uppercase letters denote matrices, unless otherwise stated. For matrix norms, $\|\mathbf{A}\|_F$ is the Frobenius norm of matrix \mathbf{A} ; $\|\mathbf{A}\|_*$ is the nuclear norm; $\|\mathbf{A}\|_2$ is the spectral norm; $\|\mathbf{A}\|_1$ is the sum of absolute values of all matrix elements; and $\|\mathbf{A}\|_\infty$ is the maximum absolute value among all matrix entries. Moreover, $\langle \mathbf{A}, \mathbf{B} \rangle$ represents $\text{tr}(\mathbf{A}^T \mathbf{B})$ for real matrices \mathbf{A}, \mathbf{B} . Additionally, σ_i is the i th largest singular value of a matrix and $\sigma_j\%$ is the singular value at the j th percentile.

Suppose that there is a matrix $\mathbf{L}_0 \in \mathbb{R}^{n_1 \times n_2}$ with rank $r \ll \min(n_1, n_2)$ and a sparse matrix $\mathbf{S}_0 \in \mathbb{R}^{n_1 \times n_2}$ with arbitrary magnitude. If we are provided with the data matrix

$$\mathbf{M} = \mathbf{L}_0 + \mathbf{S}_0, \quad (1)$$

and additional side information, how can we recover the low-rank component \mathbf{L} and the sparse noise \mathbf{S} accurately by taking advantage of the side information?

One the first methods for incorporating side information was proposed in [7] in the context of deformable face alignment. Its Low-Rank Representation algorithm (LRR) assumes that we have available an orthogonal column space $\mathbf{C} \in \mathbb{R}^{n_1 \times d_1}$, where $d_1 \leq n_1$, and

$$\begin{aligned} & \underset{\mathbf{G}, \mathbf{S}}{\text{minimise}} \quad \|\mathbf{G}\|_* + \lambda \|\mathbf{S}\|_1 \\ & \text{subject to } \mathbf{C}\mathbf{G} + \mathbf{S} = \mathbf{M}. \end{aligned} \quad (2)$$

A generalisation of the above was proposed as Principal Component Pursuit with Features (PCPF) in [17] where column $\mathbf{X} \in \mathbb{R}^{n_1 \times d_1}$ and row spaces $\mathbf{Y} \in \mathbb{R}^{n_2 \times d_2}$ were assumed to be available, where $d_2 \leq n_2$, and

$$\begin{aligned} & \underset{\mathbf{H}, \mathbf{S}}{\text{minimise}} \quad \|\mathbf{H}\|_* + \lambda \|\mathbf{S}\|_1 \\ & \text{subject to } \mathbf{X}\mathbf{H}\mathbf{Y}^T + \mathbf{S} = \mathbf{M}. \end{aligned} \quad (3)$$

The main drawback of the above mentioned models is that the side information needs to be accurate and noiseless, which is not trivial in practical scenarios.

3. Robust Principal Component Analysis Using Side Information

In this section, we propose our approach which is inspired by the use of side information in compressed sensing. In particular we will assume that we have available a noisy estimate of the low-rank component of the data $\mathbf{W} \in \mathbb{R}^{n_1 \times n_2}$. Furthermore, in order to allow use of features, we propose a methodology that allows the use of row and column orthogonal spaces \mathbf{X}, \mathbf{Y} .

3.1. The PCPS model

By encoding the side information as a structure regulariser in the sense of trace distance [28], we propose the following model of PCP using side information (abbreviated to PCPS):

$$\begin{aligned} & \underset{\mathbf{L}, \mathbf{S}}{\text{minimise}} \quad \|\mathbf{L}\|_* + \kappa \|\mathbf{L} - \mathbf{W}\|_* + \lambda \|\mathbf{S}\|_1 \\ & \text{subject to } \mathbf{L} + \mathbf{S} = \mathbf{M}, \end{aligned} \quad (4)$$

where $\kappa > 0, \lambda > 0$ are parameters that weigh the effects of side information and noise sparsity.

The proposed PCPS can be revamped to generalise the previous attempt of PCPF by the following objective of PCPS with features (PCPSF):

$$\begin{aligned} & \underset{\mathbf{H}, \mathbf{S}}{\text{minimise}} \quad \|\mathbf{H}\|_* + \kappa \|\mathbf{H} - \mathbf{D}\|_* + \lambda \|\mathbf{S}\|_1 \\ & \text{subject to } \mathbf{X}\mathbf{H}\mathbf{Y}^T + \mathbf{S} = \mathbf{M}, \quad \mathbf{X}\mathbf{D}\mathbf{Y}^T = \mathbf{W}, \end{aligned} \quad (5)$$

where $\mathbf{H} \in \mathbb{R}^{d_1 \times d_2}, \mathbf{D} \in \mathbb{R}^{d_1 \times d_2}$ are bilinear mappings for the recovered low-rank matrix \mathbf{L} and side information \mathbf{W} respectively as introduced in [19]. Note that the low-rank matrix \mathbf{L} is recovered from the optimal solution $(\mathbf{H}^*, \mathbf{S}^*)$ to objective (5) via $\mathbf{L} = \mathbf{X}\mathbf{H}^*\mathbf{Y}^T$. If side information \mathbf{W} is not available, PCPSF reduces to PCPF by setting κ to zero. If the features \mathbf{X}, \mathbf{Y} are not present either, PCP can be restored by fixing both of them at identity. However, when only the side information \mathbf{W} is accessible, objective (5) is transformed back into PCPS.

3.2. The algorithm

If we substitute \mathbf{E} for $\mathbf{H} - \mathbf{D}$ and orthogonalise \mathbf{X} and \mathbf{Y} , the optimisation problem (5) is identical to the following convex but non-smooth problem:

$$\begin{aligned} & \underset{\mathbf{H}, \mathbf{S}}{\text{minimise}} \quad \|\mathbf{H}\|_* + \kappa \|\mathbf{E}\|_* + \lambda \|\mathbf{S}\|_1 \\ & \text{subject to } \mathbf{X}\mathbf{H}\mathbf{Y}^T + \mathbf{S} = \mathbf{M}, \quad \mathbf{E} - \mathbf{H} = -\mathbf{X}^T \mathbf{W} \mathbf{Y}, \end{aligned} \quad (6)$$

which is amenable to the multi-block alternating direction method of multipliers (ADMM) as used in [27].

The corresponding augmented Lagrangian of (6) is:

$$\begin{aligned} l(\mathbf{H}, \mathbf{E}, \mathbf{S}, \mathbf{Z}, \mathbf{N}) &= \|\mathbf{H}\|_* + \kappa \|\mathbf{E}\|_* + \lambda \|\mathbf{S}\|_1 \\ &+ \langle \mathbf{Z}, \mathbf{M} - \mathbf{S} - \mathbf{XHY}^T \rangle + \frac{\mu}{2} \|\mathbf{M} - \mathbf{S} - \mathbf{XHY}^T\|_F^2 \\ &+ \langle \mathbf{N}, \mathbf{H} - \mathbf{E} - \mathbf{X}^T \mathbf{WY} \rangle + \frac{\mu}{2} \|\mathbf{H} - \mathbf{E} - \mathbf{X}^T \mathbf{WY}\|_F^2, \end{aligned} \quad (7)$$

where $\mathbf{Z} \in \mathbb{R}^{n_1 \times n_2}$ and $\mathbf{N} \in \mathbb{R}^{d_1 \times d_2}$ are Lagrange multipliers and μ is the learning rate.

The ADMM operates by carrying out repeated cycles of updates till convergence. During each cycle, $\mathbf{H}, \mathbf{E}, \mathbf{S}$ are updated serially by minimising (7) with other variables fixed. Afterwards, Lagrange multipliers \mathbf{Z}, \mathbf{N} are updated at the end of each iteration. Direct solutions to the single variable minimisation subproblems rely on the shrinkage and the singular value thresholding operators [9]. Let $\mathcal{S}_\tau(a) \equiv \text{sgn}(a) \max(|a| - \tau, 0)$ serve as the shrinkage operator, which naturally extends to matrices, $\mathcal{S}_\tau(\mathbf{A})$, by applying it to matrix \mathbf{A} element-wise. Similarly, let $\mathcal{D}_\tau(\mathbf{A}) \equiv \mathbf{U} \mathcal{S}_\tau(\Sigma) \mathbf{V}^T$ be the singular value thresholding operator on real matrix \mathbf{A} , with $\mathbf{A} = \mathbf{U} \Sigma \mathbf{V}^T$ being the singular value decomposition (SVD) of \mathbf{A} .

Minimising (7) w.r.t. \mathbf{H} at fixed $\mathbf{E}, \mathbf{S}, \mathbf{Z}, \mathbf{N}$ is equivalent to the following:

$$\arg \min_{\mathbf{H}} \|\mathbf{H}\|_* + \mu \|\mathbf{P} - \mathbf{XHY}^T\|_F^2, \quad (8)$$

where $\mathbf{P} = \frac{1}{2}(\mathbf{M} - \mathbf{S} + \mathbf{W} + \frac{1}{\mu} \mathbf{Z} + \mathbf{X}(\mathbf{E} - \frac{1}{\mu} \mathbf{N}) \mathbf{Y}^T)$. Its solution is shown to be $\mathbf{X}^T \mathcal{D}_{\frac{1}{2\mu}}(\mathbf{P}) \mathbf{Y}$. Furthermore, for \mathbf{E} ,

$$\arg \min_{\mathbf{E}} l = \arg \min_{\mathbf{E}} \kappa \|\mathbf{E}\|_* + \frac{\mu}{2} \|\mathbf{Q} - \mathbf{E}\|_F^2, \quad (9)$$

where $\mathbf{Q} = \mathbf{H} - \mathbf{X}^T \mathbf{WY} + \frac{1}{\mu} \mathbf{N}$, whose update rule is $\mathcal{D}_{\frac{\kappa}{\mu}}(\mathbf{Q})$, and for \mathbf{S} ,

$$\arg \min_{\mathbf{S}} l = \arg \min_{\mathbf{S}} \lambda \|\mathbf{S}\|_1 + \frac{\mu}{2} \|\mathbf{R} - \mathbf{S}\|_F^2, \quad (10)$$

where $\mathbf{R} = \mathbf{M} - \mathbf{XHY}^T + \frac{1}{\mu} \mathbf{Z}$ with a closed-form solution $\mathcal{S}_{\lambda\mu^{-1}}(\mathbf{R})$. Finally, Lagrange multipliers are updated as usual:

$$\mathbf{Z} = \mathbf{Z} + \mu(\mathbf{M} - \mathbf{S} - \mathbf{XHY}^T), \quad (11)$$

$$\mathbf{N} = \mathbf{N} + \mu(\mathbf{H} - \mathbf{E} - \mathbf{X}^T \mathbf{WY}). \quad (12)$$

The overall algorithm is summarised in Algorithm 1.

3.3. Complexity and convergence

Orthogonalisation of the features \mathbf{X}, \mathbf{Y} via the Gram-Schmidt process has an operation count of $O(n_1 d_1^2)$ and $O(n_2 d_2^2)$ respectively. The \mathbf{H} update in Step 4 is the most costly step of each iteration in Algorithm 1. Specifically,

Algorithm 1 ADMM solver for PCPSF

Input: Observation \mathbf{M} , side information \mathbf{W} , features \mathbf{X}, \mathbf{Y} , parameters $\kappa, \lambda > 0$, scaling ratio $\alpha > 1$.

- 1: **Initialize:** $\mathbf{Z} = 0, \mathbf{N} = \mathbf{E} = \mathbf{H} = 0, \mu = \frac{1}{\|\mathbf{M}\|_2}$.
- 2: **while** not converged **do**
- 3: $\mathbf{S} = \mathcal{S}_{\lambda\mu^{-1}}(\mathbf{M} - \mathbf{XHY}^T + \frac{1}{\mu} \mathbf{Z})$
- 4: $\mathbf{H} = \mathbf{X}^T \mathcal{D}_{\frac{1}{2\mu}}(\frac{1}{2}(\mathbf{M} - \mathbf{S} + \mathbf{W} + \frac{1}{\mu} \mathbf{Z} + \mathbf{X}(\mathbf{E} - \frac{1}{\mu} \mathbf{N}) \mathbf{Y}^T)) \mathbf{Y}$
- 5: $\mathbf{E} = \mathcal{D}_{\kappa\mu^{-1}}(\mathbf{H} - \mathbf{X}^T \mathbf{WY} + \frac{1}{\mu} \mathbf{N})$
- 6: $\mathbf{Z} = \mathbf{Z} + \mu(\mathbf{M} - \mathbf{S} - \mathbf{XHY}^T)$
- 7: $\mathbf{N} = \mathbf{N} + \mu(\mathbf{H} - \mathbf{E} - \mathbf{X}^T \mathbf{WY})$
- 8: $\mu = \mu \times \alpha$
- 9: **end while**

Return: $\mathbf{L} = \mathbf{XHY}^T, \mathbf{S}$

the SVD required in the singular value thresholding action dominates with $O(\min(n_1 n_2^2, n_1^2 n_2))$ complexity.

It has been recently established that for a 3-block separable convex minimisation problem, the direct extension of the ADMM achieves global convergence with linear convergence rate if one block in the objective is sub-strongly monotonic [13]. In our case, it can be shown that $\|\mathbf{S}\|_1$ processes such sub-strong monotonicity. We have also used the fast continuation technique already applied to the matrix completion problem [18] to increase μ incrementally for accelerated superlinear performance [22]. The cold start initialisation strategies for variables \mathbf{H}, \mathbf{E} and Lagrange multipliers \mathbf{Z}, \mathbf{N} are described in [4]. Besides, we have scheduled \mathbf{S} to be updated first and taken the initial learning rate μ as suggested in [29]. As for stopping criteria, we have employed the Karush-Kuhn-Tucker (KKT) feasibility conditions. Namely, within a maximum number of 1000 iterations, when the maximum of $\|\mathbf{M} - \mathbf{S}_k - \mathbf{XH}_k \mathbf{Y}^T\|_F / \|\mathbf{M}\|_F$ and $\|\mathbf{H}_k - \mathbf{E}_k - \mathbf{X}^T \mathbf{WY}\|_F / \|\mathbf{M}\|_F$ dwindle from a pre-defined threshold ϵ , the algorithm is terminated, where k signifies values at the k^{th} iteration.

4. Experimental results

In this section, we illustrate the enhancement made by side information through both numerical simulations and real-world applications. First, we explain how parameters used in our implementation are tuned. Second, we compare the recoverability of our proposed PCPSF algorithm with state-of-the-art methods for incorporating features or dictionary, viz. PCPF [17] and LRR [11] on synthetic data as well as the baseline PCP [9] when there are no features available. Third, we show how powerful side information can be for the task of object segmentation in video pre-processing. Fourth, we demonstrate that side information is instructive in the low-dimensionality face modeling from images of different illuminations. Last, we reveal that the more ac-

curately reconstructed expressions in the light of side information lead to better emotion classification, for which we also include Partial Sum of Singular Values (PSSV) [25] in our comparison for its stated advantage in view of the limited number of expression observations available.

For LRR, clean subspace \mathbf{X} is used as in [7] instead of the observation \mathbf{M} itself as the dictionary. PCP is solved via the inexact ALM [29] and the heuristics for predicting the dimension of principal singular space is not adopted here due to its lack of validity on uncharted real data [20]. The stopping criteria for PCPF, LRR, PCP and PSSV are all set to KKT optimality conditions for reasons of consistency.

4.1. Parameter calibration

In order to tune the algorithmic parameters, we first conduct a benchmark experiment as follows: a low-rank matrix \mathbf{L}_0 is generated from $\mathbf{L}_0 = \mathbf{JK}^T$, where $\mathbf{J}, \mathbf{K} \in \mathbb{R}^{200 \times 10}$ have entries from a $\mathcal{N}(0, 0.005)$ distribution; a 200×200 sparse matrix \mathbf{S}_0 is generated by randomly setting 38,000 entries to zero with others taking values of ± 1 with equal probability; side information \mathbf{W} is assumed perfect, that is, $\mathbf{W} = \mathbf{L}_0$; \mathbf{X} is set as the left-singular vectors of \mathbf{L}_0 ; and \mathbf{Y} is set as the right-singular vectors of \mathbf{L}_0 . It has been found that a scaling ratio $\alpha = 1.1$, a tolerance threshold $\epsilon = 10^{-7}$ and a maximum step size $\mu = 10^{18}$ to avoid ill-conditioning can bring all models except PSSV to convergence with a recovered \mathbf{L} of rank 10, a recovered \mathbf{S} of sparsity 5% and an accuracy $\|\mathbf{L} - \mathbf{L}_0\|_F/\|\mathbf{L}_0\|_F$ on the order of 10^{-6} . Still, these apply to PSSV as is done similarly in [25].

Although theoretical determination of κ and λ is beyond the scope of this paper, we nevertheless provide empirical guidance based on extensive experiments. A parameter sweep in the $\kappa - \lambda$ space for perfect side information is shown in Figure 1(a) and for observation as side information in Figure 1(b) to impart a lower bound and an upper bound respectively. It can be easily seen that $\lambda = 1/\sqrt{200}$ (or $\lambda = 1/\sqrt{\max(n_1, n_2)}$) for a general matrix of dimension $n_1 \times n_2$ from Robust PCA works well in both cases. Conversely, κ depends on the quality of the side information.

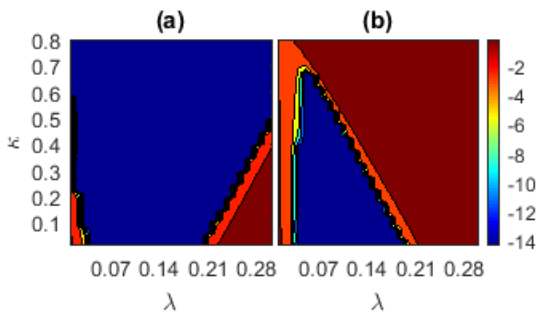


Figure 1: Log-scale relative error ($\log \frac{\|\mathbf{L} - \mathbf{L}_0\|_F}{\|\mathbf{L}_0\|_F}$) of PCPS (a) when side information is perfect ($\mathbf{W} = \mathbf{L}_0$) and (b) when side information is the observation ($\mathbf{W} = \mathbf{M}$).

When the side information is accurate, a large κ should be selected to capitalise upon the side information as much as possible, whereas when the side information is improper, a small κ should be picked to sidestep the dissonance caused by the side information. Here, we have discovered that a κ value of 0.2 works best with synthetic data and a value of 0.5 is suited for public video sequences, both of which will be used in all experiments in subsequent sections together with other aforementioned parameter settings. It is worth emphasising again that prior knowledge of the structural information about the data yields more appropriate values for κ and λ .

4.2. Phase transition on synthetic datasets

We now focus on the recoverability problem, *i.e.* recovering matrices of varying ranks from errors of varying sparsity. True low-rank matrices are created via $\mathbf{L}_0 = \mathbf{JK}^T$, where $200 \times r$ matrices \mathbf{J}, \mathbf{Y} have independent elements drawn randomly from a Gaussian distribution of mean 0 and variance $5 \cdot 10^{-3}$ so r is the rank of \mathbf{L}_0 . Next, we generate 200×200 error matrices \mathbf{S}_0 , which possess $\rho_s \cdot 200^2$ non-zero elements located randomly within the matrix. We consider two types of entries for \mathbf{S}_0 : Bernoulli ± 1 and $\mathcal{P}_\Omega(\text{sgn}(\mathbf{L}_0))$, where \mathcal{P} is the projection operator and Ω is the support set of \mathbf{S}_0 . $\mathbf{M} = \mathbf{L}_0 + \mathbf{S}_0$ thus becomes the simulated observation. For each (r, ρ_s) pair, three observations are constructed. The recovery is successful if for all these three problems,

$$\frac{\|\mathbf{L} - \mathbf{L}_0\|_F}{\|\mathbf{L}_0\|_F} < 10^{-3} \quad (13)$$

from the recovered \mathbf{L} . In addition, let $\mathbf{L}_0 = \mathbf{U}\Sigma\mathbf{V}^T$ be the SVD of \mathbf{L}_0 . Feature \mathbf{X} is formed by randomly interweaving column vectors of \mathbf{U} with d arbitrary orthonormal bases for the null space of \mathbf{U}^T , while permuting the expanded columns of \mathbf{V} with d random orthonormal bases for the kernel of \mathbf{V}^T forms feature \mathbf{Y} . Hence, the feasibility conditions are fulfilled: $\mathbb{C}(\mathbf{X}) \supseteq \mathbb{C}(\mathbf{L}_0)$, $\mathbb{C}(\mathbf{Y}) \supseteq \mathbb{C}(\mathbf{L}_0^T)$, where \mathbb{C} is the column space operator.

Entry-wise corruptions. For these trials, we construct the side information by directly adding small Gaussian noise to each element of \mathbf{L}_0 : $l_{ij} \rightarrow l_{ij} + \mathcal{N}(0, 2.5r \cdot 10^{-9})$, $i, j = 1, 2, \dots, 200$. As a result, the standard deviation of the error in each element is 1% of that among the elements themselves. On average, the Frobenius percent error, $\|\mathbf{W} - \mathbf{L}_0\|_F/\|\mathbf{L}_0\|_F$, is 1%. Such side information is genuine in regard to the fact that classical PCA with accurate rank is not able to eliminate the noise [3]. For $d = 10$, Figures 2(a.I) and 2(a.II) plot results from PCPF, LRR and PCPSF. On the other hand, the situation with no available features is investigated in Figures 2(a.III) and 2(a.IV) for PCP and PCPS. The frontier of PCPF has been advanced by PCPSF everywhere for both sign types. Especially at

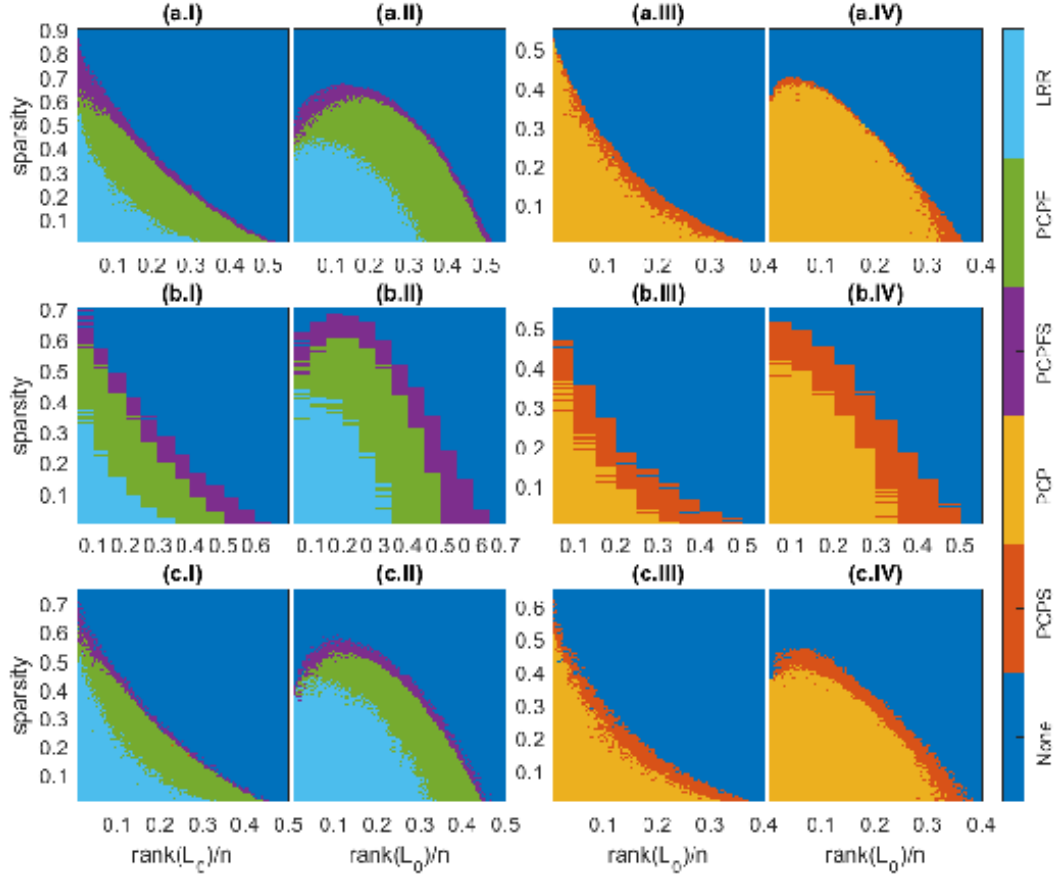


Figure 2: Domains of recovery by various algorithms: **(I,III)** for random signs and **(II,IV)** for coherent signs. **(a)** for entry-wise corruptions, **(b)** for deficient ranks and **(c)** for distorted singular values.

low ranks, errors with much higher density can be removed. Without features, PCPS surpasses PCP by and large with significant expansion at small sparsity for both cases.

Deficient ranks. Now we first make a new matrix Σ' by retaining only the singular values from σ_1 to $\sigma_{90\%}$ in Σ . Then, side information is constructed according to $\mathbf{W} = \mathbf{U}\Sigma'\mathbf{V}^T$, aka hard thresholding. As rank increases, Frobenius percent error of \mathbf{W} decreases from 23.3% to 5.8% sub-linearly. Figures 2(b.I) and 2(b.II) show results from PCPF, LRR and PCPSF where d is again kept at 10. The corresponding cases with no features are presented in Figures 2(b.III) and 2(b.IV) for PCP and PCPS. Notwithstanding the most spurious side information, PCPSF and PCPS have reclaimed the largest region unattainable by PCPF and PCP respectively for the two signs.

Distorted singular values. Here, we produce the matrix Σ' by adding Gaussian noise to singular values in Σ : $\sigma_i \rightarrow \sigma_i + 0.01 \cdot \mathcal{N}(0, \sigma_i^2)$ for all i . Next, side information is formed by $\mathbf{W} = \mathbf{U}\Sigma'\mathbf{V}^T$. The mean Frobenius percent error in \mathbf{W} is 1%. With d relaxed to 50, recoverability diagrams for PCPF, LRR, PCPSF and PCP, PCPS are drawn in Figures (c.I), (c.II) and (c.III), (c.IV). We observe substan-

tial growth of recoverability for PCPS over PCP across the full range of ranks. And with features, there is still omniscient gain in recoverability for PCPSF against PCPF, which is marked at low ranks.

We remark that in unrecoverable areas, PCPS and PCPSF still obtain much smaller values of $\|\mathbf{L} - \mathbf{L}_0\|_F$. In view of the marginal improvement of LRR contrasted with PCPF and PCPSF, we will not consider it any longer.

4.3. Face denoising under variable illumination

It has been previously proved that a convex Lambertian surface under distant and isotropic lighting has an underlying model that spans a 9-D linear subspace [23]. Albeit faces can be described as Lambertian, it is only approximate and harmonic planes are not real images due to negative pixels. In addition, theoretical lighting conditions cannot be realised and there are unavoidable occlusion and albedo variations. It is thus more natural to decompose facial image formation as a low-rank component for face description and a sparse component for defects. What is more, we suggest that further boost to the performance of facial characterisation can be gained by leveraging an image which faithfully



Figure 3: Comparison of face denoising ability by various state-of-art methods: The first row contains sample frames from subject 2 and subject 33 with side information shown to the right. For other rows, faces recovered from PCP are shown in (a), PCPF in (b), PCPS in (c) and PCPSF in (d). Rows 2,3 are for single person experiments and row 4 corresponds to the multiperson experiment.

represents the subject.

We consider images of a fixed pose under different illuminations from the extended Yale B database for testing. Ten subjects were randomly chosen and all 64 images were studied for each person. For single-person experiments, 32556×64 observation matrices were formed by vectorising each 168×192 image and the side information was chosen to be the average of all images, tiled to the same size as the observation matrix for each subject. For the multiperson experiment, both single-person observation and side information matrices were concatenated into 32556×640 matrices respectively.

For PCPF and PCPSF to run, we learn the feature dictionary following an approach by Vishal *et al.* [26]. In a nutshell, the feature learning process can be treated as a sparse encoding problem. More specifically, we simultaneously seek a dictionary $\mathbf{D} \in \mathbb{R}^{n_1 \times c}$ and a sparse representation $\mathbf{B} \in \mathbb{R}^{c \times n_2}$ such that:

$$\begin{aligned} & \underset{\mathbf{D}, \mathbf{B}}{\text{minimise}} \quad \|\mathbf{M} - \mathbf{DB}\|_F^2 \\ & \text{subject to} \quad \gamma_i \leq t \quad \text{for } i = 1 \dots n_2, \end{aligned} \quad (14)$$

where c is the number of atoms, γ_i 's count the number of non-zero elements in each sparsity code and t is the sparsity constraint factor. This can be solved by the K-SVD algorithm [1]. Here, feature \mathbf{X} is the dictionary \mathbf{D} , feature \mathbf{Y} corresponds to a similar solution using the transpose of the observation matrix as input and the sparse codes are irrelevant. For implementation details, we set c to 40, t to 40 and used 10 iterations. Because K-SVD could not converge in reasonable time for the multiperson experiment, we resorted to classical PCA applied to the observation matrix to obtain features \mathbf{X}, \mathbf{Y} of dimension 400.

As a visual illustration, two challenging cases are exhibited in Figure 3. For subject 2, it is clearly evident that PCPS and PCPSF outperform the best existing methods through the complete elimination of acquisition faults. More surprisingly, PCPSF even manages to restore the flash in the pupils that is not present in the side information. For subject 33, PCPS indubitably reconstructs a more vivid left eye than that from PCP which is only discernible. With that said, PCPSF still prevails by uncovering more shadows, especially around the medial canthus of the left eye, and revealing a more distinct crease in the upper eyelid as well a more translucent iris. We also notice that results from the single-person experiment outdo their counterparts from the multiperson experiment. Thence, we will focus on a single subject alone. To quantitatively verify the improvement made by our proposed approach, we examine the structural information contained within the denoised eigenfaces. Singular values of the recovered low-rank matrices from all algorithms are plotted in Figure 4. Singular values decrease most sharply for PCPSF followed by PCPS. By the theoretical limit, they are orders of magnitude smaller than those

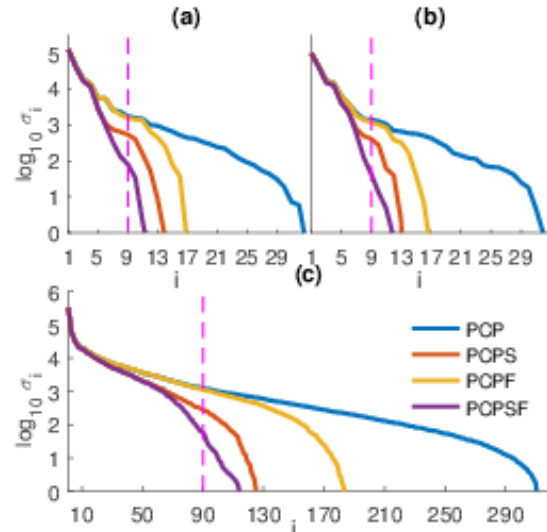


Figure 4: Log-scale singular values of the denoised matrices for subject 2 in (a), for subject 33 in (b) and for all subjects in (c).



Figure 5: Background subtraction results for two sample frames: In row 1, (a,c) are original images from PETS and airport respectively, with corresponding ground truth in (b,d). Row 2 encompasses outcomes from PCP and row 3 from PCPS, together with recovered background in columns (a,c) and foreground in (b,d).

values from other methods. This validates our proposed approaches.

4.4. Background subtraction from surveillance video

In automated video analytics, object detection is instrumental in object tracking, activity recognition and behaviour understanding. Practical applications include surveillance, traffic control, robotic operation, etc., where foreground objects can be people, vehicles, products and so forth. Background subtraction segments moving objects by calculating the pixel-wise difference between each video frame and the background. For a static camera, the background is almost static, while the foreground objects are mostly moving. Consequently, a decomposition into a low-rank component for the background and a sparse component for foreground objects is a valid model for such dynamics. Indeed, if the only change in the background is illumination, then the matrix representation of vectorised backgrounds has a rank of 1. It has been demonstrated that Robust PCA is quite effective for such a low-rank matrix analysis problem [9]. Nevertheless, through the application of our proposed algorithm to such a background-foreground separation scenario, we show that useful side information can help achieve better background restoration.

One video sequence from the PETS 2006 dataset and one from the I2R dataset were utilised for evaluation. Each consists of scenes at a hall where people walk intermittently.

200 consecutive frames of 720×576 resolution grayscale images were stacked by columns into a 414720×200 observation matrix from the first video and 200 frames of 176×144 images from the second video were stacked into another 25344×200 observation matrix. Two side information arrays comprised columns that are copies of a vectorised photo which contains an empty hallway. To commence object detection, PCP and PCPS were first run to extract the backgrounds. Then objects were recovered by calculating the absolute values of the difference between the original frame and the estimated background. Since parameters for dictionary learning need exhaustive search, we will not be comparing PCPF and PCPSF for what follows. We quantitatively compare the performance of the competing methods according to the weighted F-measure [21] against manually annotated bounding boxes provided as the ground

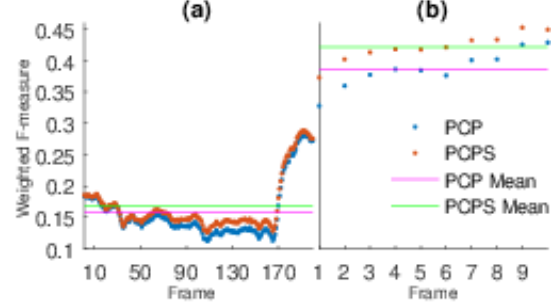


Figure 6: Weighted F-measure scores of PCP and PCPS for each frame of PETS in (a) and Airport in (b).

truth. The resulting scatter plots for the frames are presented in Figure 6. From the consistently higher precision statistics, the merit of PCPS over PCP is confirmed. For qualitative reference, representative images of the recovered background and foreground from the two methods are listed in Figure 5. PCP only partially detects infrequent moving objects, people who stop moving for extended periods of time, leaving ghost artifacts in the background. In contrast, PCPS segments a fairly sharp silhouette of slowly moving objects to produce a much cleaner background, promoting its novelty.

4.5. Face and facial expression recognition

Recent research has established that an expressive face can be treated as a neutral face plus a sparse expression component [24], which is identity-independent due to its constituent local non-rigid motions, *i.e.* action units. This is central to computer vision as it enables human emotion classification from such visual cues. We will demonstrate how the accurate reconstruction of facial expressions guided by side information ameliorates classification analysis.

To begin with, evaluation was effected on the CMU Multi-PIE dataset. Aligned and cropped 165×172 images of frontal pose and normal lighting from 54 subjects were used. We batch-processed each subject forming a 28380×6 observation matrix to extract expressions: Neutral, Smile, Surprise, Disgust, Scream and Squint. For each subject,



Figure 7: Expression extraction for a single subject: Expressive faces reside in row 1. Identity classes produced by PCP, PSSV, PCPS are in rows 2, 4, 6. The complementary expression components are depicted in rows 3, 5, 7.

side information was offered by a sextet of neutral face repetitions. Archetypal expressions recovered by PCP, PCPS, PSSV (rank 1) are laid out in Figure 7. It is noteworthy that local appearance changes separated by PCPS are the most salient which paves the way for better classification. We avail ourselves of the multi-class RBF-kernel SVM [5] and the SRC [14] to map expressions to emotions. 9-fold cross-validation results are reported in Table 1. PCPS leads PCP by a fair margin with PSSV performing the worst.

Algorithm	Non-linear SVM	SRC
PCP	78.40%	79.01%
PSSV	74.69%	74.38%
PCPS	79.94%	82.72%

Table 1: Classification accuracy on the Multi-PIE dataset for PCP, PSSV and PCPS by means of Nonlinear SVM and SRC learning.

Lastly, the CK+ dataset was incorporated to assess the joint face and expression recognition capabilities of various algorithms. Each test image is sparsely coded via a dictionary of both identities and universal expressions (Anger, Disgust, Fear, Happiness, Sadness and Surprise). The least resulting reconstruction residual thereupon determines its identity or expression. We refer readers to [6] for the exact problem set-up and implementation details. Table 2 collects the computed recognition rates. PSSV turns out inferior to all others and PCPS performs distinctly better than PCP.

Algorithm	Identity	Expression
PCP	87.35%	49.24%
PSSV	87.05%	45.30%
PCPS	95.23%	67.50%

Table 2: Recognition rates for joint identity & expression recognition averaged over 10 trials on CK+

5. Conclusion

In this paper, we have, for the first time, assimilated side information of the same format as observation into the framework of Robust Principle Component Analysis based on trace norms. Existing extensions of subspace features have also been successfully amalgamated in a convex fashion. Extensive experiments have shown that our algorithms not only perform better where Robust PCA is effective but also remain potent when Robust PCA fails. Directions for future research include generalising to the tensor case and to components of multiple scales.

References

- [1] M. Aharon, M. Elad, and A. Bruckstein. K -svd: An algorithm for designing overcomplete dictionaries for sparse representation. *IEEE Transactions on Signal Processing*, 54(11):4311–4322, 2006. 6

[2] A. Aleksandr, B. Stephen, C. Volkan, and O. Peder. A variational approach to stable principal component pursuit. *Proceedings of the Thirtieth Conference Conference on Uncertainty in Artificial Intelligence*, pages 32–41, 2014. 1

[3] S. Andrey and N. Andrew. Reconstruction of a low-rank matrix in the presence of gaussian noise. *Journal of Multivariate Analysis*, 118:67–76, 2013. 4

[4] S. Boyd, N. Parikh, E. Chu, B. Peleato, and J. Eckstein. Distributed optimization and statistical learning via the alternating direction method of multipliers. *Foundations and Trends in Machine Learning*, 3(1):1–122, 2011. 3

[5] C. Chih-Chung and L. Chih-Jen. Libsvm: A library for support vector machines. *ACM Transactions on Intelligent Systems and Technology*, 2(3):27–27, 2011. 8

[6] G. Christos, P. Yannis, and P. Maja. Discriminant incoherent component analysis. *IEEE Transactions on Image Processing*, 25(5):2021–2034, 2016. 8

[7] S. Christos, P. Yannis, Z. Stefanos, and P. Maja. Raps: Robust and efficient automatic construction of person-specific deformable models. *IEEE Conference on Computer Vision and Pattern Recognition*, pages 1789–1796, 2014. 1, 2, 4

[8] C. Emmanuel. The restricted isometry property and its implications for compressed sensing. *Comptes Rendus Mathematique*, 346(9):589–592, 2008. 1

[9] C. Emmanuel, L. Xiaodong, M. Yi, and W. John. Robust principal component analysis? *Journal of the ACM*, 58(3):11:1–11:37, 2011. 1, 3, 7

[10] S. Fanhua, L. Yuanyuan, C. James, and C. Hong. Robust principal component analysis with missing data. *Proceedings of the 23rd ACM International Conference on Conference on Information and Knowledge Management*, pages 1149–1158, 2014. 1

[11] L. Guangcan, L. Zhouchen, Y. Shuicheng, S. Ju, Y. Yong, and M. Yi. Robust recovery of subspace structures by low-rank representation. *IEEE Transactions on Pattern Analysis and Machine Intelligence*, 35(1):171–184, 2013. 1, 3

[12] X. Huan, C. Constantine, and S. Sujay. Robust pca via outlier pursuit. *IEEE Transactions on Information Theory*, 58(5):3047–3064, 2012. 1

[13] S. Huijie, W. Jinjiang, and D. Tingquan. On the global and linear convergence of direct extension of admm for 3-block separable convex minimization models. *Journal of Inequalities and Applications*, (227):227, 2016. 3

[14] W. John, Y. Allen, G. Arvind, S. Shankar, and M. Yi. Robust face recognition via sparse representation. *IEEE Transactions on Pattern Analysis and Machine Intelligence*, 31(2):210–227, 2009. 8

[15] M. Joo, D. Nikos, and R. Miguel. Compressed sensing with side information: Geometrical interpretation and performance bounds. *IEEE Global Conference on Signal and Information Processing*, pages 512–516, 2014. 1

[16] C. Kai-Yang, H. Cho-Jui, and D. Inderjit. Matrix completion with noisy side information. *Advances in Neural Information Processing Systems 26*, pages 3447–3455, 2015. 1

[17] C. Kai-Yang, H. Cho-Jui, and D. Inderjit. Robust principal component analysis with side information. *Proceedings of The 33rd International Conference on Machine Learning*, pages 2291–2299, 2016. 1, 2, 3

[18] T. Kim-chuan and Y. Sangwoon. An accelerated proximal gradient algorithm for nuclear norm regularized least squares problems. *Pacific Journal of Optimization*, 6(3):615–640, 2010. 3

[19] X. Miao and Z. Zhi-hua. Speedup matrix completion with side information: Application to multi-label learning. *Advances in Neural Information Processing Systems 26*, pages 2301–2309, 2013. 1, 2

[20] H. Michael and W. Tao. Robust principal component pursuit via inexact alternating minimization on matrix manifolds. *Journal of Mathematical Imaging and Vision*, 51(3):361–377, 2015. 4

[21] M. Ran, Z. Lih, and T. Ayellet. How to evaluate foreground maps? *IEEE Conference on Computer Vision and Pattern Recognition*, 2014. 7

[22] R. Rockafellar. Monotone operators and the proximal point algorithm. *SIAM Journal on Control and Optimization*, 14(5):877–898, 1976. 3

[23] B. Ronen and J. D. and. Lambertian reflectance and linear subspaces. *IEEE Transactions on Pattern Analysis and Machine Intelligence*, 25(2):218–233, 2003. 5

[24] T. Sima, P. Vishal, and C. Rama. Component-based recognition of faces and facial expressions. *IEEE Transactions on Affective Computing*, 4:360–371, 2013. 8

[25] O. Tae-Hyun, T. Yu-Wing, B. Jean-Charles, K. Hyeongwoo, and K. I. So. Partial sum minimization of singular values in robust pca: Algorithm and applications. *IEEE TRANSACTIONS ON PATTERN ANALYSIS AND MACHINE INTELLIGENCE*, 38(4):744–758, 2016. 4

[26] P. Vishal, W. Tao, B. Soma, P. Jonathon, and C. Rama. Dictionary-based face recognition under variable lighting and pose. *IEEE Transactions on Information Forensics and Security*, 7(3):954–965, 2012. 6

[27] P. Yannis, N. Mihalis, Z. Stefanos, and P. Maja. Robust correlated and individual component analysis. *Journal of Inequalities and Applications*, 38(8):1665–1678, 2016. 2

[28] L. Zhang and V. Lieven. Interior-point method for nuclear norm approximation with application to system identification. *SIAM Journal on Matrix Analysis and Applications*, 31(3):1235–1256, 2009. 2

[29] L. Zhuocheng, C. Minming, and M. Yi. The augmented lagrange multiplier method for exact recovery of corrupted low-rank matrices. *UIUC Technical Report*, 2009. 3, 4

[30] Z. Zihan, L. Xiaodong, W. John, C. Emmanuel, and M. Yi. Stable principal component pursuit. *IEEE International Symposium on Information Theory Proceedings*, pages 1518–1522, 2010. 1